

Thermal entanglement in a spin-1/2 Ising-Heisenberg butterfly-shaped chain with impurities

Meng-Ru Ma(马梦如), Yi-Dan Zheng(郑一丹), Zhu Mao(毛竹), Bin Zhou(周斌)

Citation: Chin. Phys. B . 2020, 29(11): 110308 . **doi:** 10.1088/1674-1056/abbbde
Journal homepage: http://cpb.iphy.ac.cn; http://iopscience.iop.org/cpb

What follows is a list of articles you may be interested in

Entanglement teleportation via a couple of quantum channels in Ising-Heisenberg spin chain model of a heterotrimetallic Fe-Mn-Cu coordination polymer

Yi-Dan Zheng(郑一丹), Zhu Mao(毛竹), Bin Zhou(周斌)

Chin. Phys. B . 2019, 28(12): 120307 . **doi:** 10.1088/1674-1056/ab53cc

Thermal quantum correlations of a spin-1/2 Ising-Heisenberg diamond chain with Dzyaloshinskii-Moriya interaction

Yidan Zheng(郑一丹), Zhu Mao(毛竹), Bin Zhou(周斌)

Chin. Phys. B . 2018, 27(9): 090306 . **doi:** 10.1088/1674-1056/27/9/090306

Thermal entanglement of the spin-1 Ising–Heisenberg diamond chain with biquadratic interaction

Yi-Dan Zheng(郑一丹), Zhu Mao(毛竹), Bin Zhou(周斌)

Chin. Phys. B . 2017, 26(7): 070302 . **doi:** 10.1088/1674-1056/26/7/070302

Thermal entanglement of the Ising–Heisenberg diamond chain with Dzyaloshinskii–Moriya interaction

Qiao Jie, Zhou Bin

Chin. Phys. B . 2015, 24(11): 110306 . **doi:** 10.1088/1674-1056/24/11/110306

Entangled quantum heat engine based on two-qubit Heisenberg *XY* model

He Ji-Zhou,He Xian,Zheng Jie

Chin. Phys. B . 2012, 21(5): 050303 . **doi:** 10.1088/1674-1056/21/5/050303

Thermal entanglement in a spin-1/2 Ising–Heisenberg butterfly-shaped chain with impurities*

Meng-Ru Ma(马梦如), Yi-Dan Zheng(郑一丹), Zhu Mao(毛竹)†, and Bin Zhou(周斌)‡

Department of Physics, Hubei University, Wuhan 430062, *China*

(Received 13 August 2020; revised manuscript received 1 September 2020; accepted manuscript online 2020)

We investigate the effect of impurities on the thermal entanglement in a spin-1/2 Ising–Heisenberg butterfly-shaped chain, where four interstitial Heisenberg spins are localized on the vertices of a rectangular plaquette in a unit block. By using the transfer-matrix approach, we numerically calculate the partition function and the reduced density matrix of this model. The bipartite thermal entanglement between different Heisenberg spin pairs is quantified by the concurrence. We also discuss the fluctuations caused by the impurities through the uniform distribution and the Gaussian distribution. Considering the effects of the external magnetic field, temperature, Heisenberg and Ising interactions as well as the parameter of anisotropy on the thermal entanglement, our results show that comparing with the case of the clean model, in both the two-impurity model and the impurity fluctuation model the entanglement is more robust within a certain range of anisotropic parameters and the region of the magnetic field where the entanglement occurred is also larger.

Keywords: thermal entanglement, Ising–Heisenberg butterfly-shaped chain, impurities, transfer-matrix approach

PACS: 03.67.Bg, 03.67.Mn, 75.10.Pq **DOI:** 10.1088/1674-1056/abbbde

1. Introduction

The existence of quantum entanglement has been found in the early period due to the peculiar non-locality of quantum mechanics and confirmed by many experiments.[1,2] With the rapid development of quantum information science, it is now possible to achieve quantum information processing like quantum teleportation,[3–5] quantum key distribution,[6–8] and quantum cloning[9–11] through quantum entanglement resource. It is worth noticing that a real physical system always exists at a finite temperature, so it is necessary to study the effect of temperature on quantum entanglement by considering the state of the system at thermal equilibrium.[12–14] Measuring entanglement is a very important research field and many different methods have been proposed to quantify entanglement measure. Wootters *et al*. proposed the concurrence as a kind of entanglement measure to quantify entanglement of formation for two-qubit systems, which is applicable to both the pure and the mixed states.[13–19]

Over the past decades, the thermal entanglement between qubits in quantum Ising coupling model, anisotropic XY and XXZ Heisenberg spin-1/2 models has been extensively studied.[20–23] And these one-dimensional models can also be solved exactly by the Bethe ansatz technique and the transfer-matrix approach.[24–26] Due to the importance of impurities in quantum systems, spin chains with impurities have attracted much attention.[27] The entangled chain with defects was proposed by introducing a single defect in the exchange interaction term of the quantum XY model.[28] In addition, the XXZ model with two defects,[29] the XXZ model with defects in the presence of external magnetic field,[30] the disorder in quantum Ising model,[31] the Gaussian disorder in quantum XY and XXZ models have also been studied to inspect the behavior of concurrence.[32,33]

In recent years, more and more attention has been paid to the study of quantum entanglement and thermodynamic properties in infinite spin chains as the models of the actual materials. Based on the researches of the natural mineral azurite $Cu_3(CO_3)_2(OH)_2$,[34,35] the Ising-XXZ diamond model has been discussed.[36,37] The one-dimensional infinite chain such as the Ising-XXZ diamond chain and the Ising-XYZ distorted diamond chain has been exactly solved for discussing the properties of thermal entanglement.[38,39] The particular spin-1/2 Ising–Heisenberg orthogonal-dimer chain with total spin on vertical Heisenberg bonds from the magnetic structure $[Dy_2Cu_2]_n$ is demonstrated to analyze the ground states and thermodynamic properties.[40] Additionally, the Ising–Heisenberg tetrahedral chain with total spin angular momentum for two spins coupled by the Heisenberg interaction are introduced to calculate the concurrence and the specific heat.[41,42] By using the star-triangle mapping transformation and the transfer-matrix approach, the spin-1/2 Ising–Heisenberg pentagonal chain is also rigorously solved

*Project supported by the National Natural Science Foundation of China (Grant No. 12074101), the Science Fund for the New Century Excellent Talents in University of the Ministry of Education of China (Grant No. NCET-11-0960), and the Specialized Research Fund for the Doctoral Program of Higher Education of China (Grant No. 20134208110001).

†Corresponding author. E-mail: maozhu@hubu.edu.cn

‡Corresponding author. E-mail: binzhou@hubu.edu.cn

© 2020 Chinese Physical Society and IOP Publishing Ltd

to investigate the bipartite quantum entanglement.[43] It is noted that the effect of impurities on the thermal entanglement of the spin-1/2 Ising-XXZ diamond chain has been investigated.[44,45]

Very recently, the magnetic properties and the specific heat in a spin-1/2 Ising–Heisenberg butterfly-shaped chain have been investigated,[46] however, up to now the thermal entanglement properties in the Ising–Heisenberg butterfly-shaped spin chain model has not been discussed yet. Thus, in this paper, we will focus on the effect of two impurities on the thermal entanglement of the intriguing Ising–Heisenberg butterfly-shaped spin chain model. We will use the transfer-matrix approach to numerically calculate the partition function and the reduced density matrix of this model. The bipartite thermal entanglement between different Heisenberg spin pairs is quantified by the concurrence. Additionally, we also introduce the impurity fluctuations with the uniform distribution and the Gaussian distribution in this spin chain model. It is found that comparing with the case of the clean model, in both the two-impurity model and the impurity fluctuation models, the thermal entanglement is more robust and the magnetic field regions the entanglement occurring are also larger within a certain range of anisotropic parameters.

The rest of this paper is organized as follows. We present the spin-1/2 Ising–Heisenberg butterfly-shaped chain model and give the exact solution via the transfer-matrix approach in Section 2. In Section 3, the interesting results for the concurrence of the clean model, the two impurities model and the impurities subject to the uniform distribution and the Gaussian distribution will be displayed, respectively. Finally, we give our conclusions in Section 4.

2. Model and method

Let us consider the quantum spin-1/2 Ising–Heisenberg butterfly-shaped chain, including four interstitial Heisenberg spins localized on the vertices of a rectangular plaquette in a unit block, the schematic of which is illustrated in Fig. 1. Spins in a rectangular plaquette of each unit block are connected through Heisenberg interactions (denoted by $(J_{\rm H},\Delta)$). The parameter J represents Ising interactions. Aiming to investigate the effect of impurities on the thermal entanglement, it is assumed that the interaction parameters are homogeneous in all unit blocks along the spin chain except the impurities block located at $r-1$ and $r+1$ in Fig. 1. Thus the total Hamiltonian can be expressed as follows:[44,45]

$$H=\sum_{i=1}^{N}H_i, \tag{1}$$

where $H_i=H_i^{\rm host}+H_i^{\rm imp}$, with

$$\begin{aligned}H_i^{\rm host}=&-\sum_{j=1}^{4}J_{\rm H}(\boldsymbol{S}_{j,i}\cdot\boldsymbol{S}_{j+1,i})_{\Delta}+J\left[(\sigma_{a,i}^z+\sigma_{a,i+1}^z)(S_{1,i}^z+S_{2,i}^z)+(\sigma_{b,i}^z+\sigma_{b,i+1}^z)(S_{3,i}^z+S_{4,i}^z)+\frac{1}{2}(\sigma_{a,i}^z\sigma_{b,i}^z+\sigma_{a,i+1}^z\sigma_{b,i+1}^z)\right]\\&-B\sum_{j=1}^{4}S_{j,i}^z-\frac{B}{2}(\sigma_{a,i}^z+\sigma_{b,i}^z+\sigma_{a,i+1}^z+\sigma_{b,i+1}^z),\end{aligned} \tag{2}$$

for $i=1,2,\ldots,r-2,r,r+2,\ldots,N$, and

$$\begin{aligned}H_i^{\rm imp}=&-\sum_{j=1}^{4}\widetilde{J}_{\rm H}(\boldsymbol{S}_{j,i}\cdot\boldsymbol{S}_{j+1,i})_{\widetilde{\Delta}}+\widetilde{J}\left[(\sigma_{a,i}^z+\sigma_{a,i+1}^z)(S_{1,i}^z+S_{2,i}^z)+(\sigma_{b,i}^z+\sigma_{b,i+1}^z)(S_{3,i}^z+S_{4,i}^z)+\frac{1}{2}(\sigma_{a,i}^z\sigma_{b,i}^z+\sigma_{a,i+1}^z\sigma_{b,i+1}^z)\right]\\&-B\sum_{j=1}^{4}S_{j,i}^z-\frac{B}{2}(\sigma_{a,i}^z+\sigma_{b,i}^z+\sigma_{a,i+1}^z+\sigma_{b,i+1}^z),\end{aligned} \tag{3}$$

for $i=r-1,r+1$. Here,

$$(\boldsymbol{S}_{j,i}\cdot\boldsymbol{S}_{j+1,i})_{\Delta}=S_{j,i}^xS_{j+1,i}^x+S_{j,i}^yS_{j+1,i}^y+\Delta S_{j,i}^zS_{j+1,i}^z,$$

corresponding to the interstitial anisotropic Heisenberg spins coupling ($J_{\rm H}$ and Δ) and $S_{5,i}=S_{1,i}$. $\widetilde{J}_{\rm H}=J_{\rm H}(1+\alpha)$, $\widetilde{\Delta}=\Delta(1+\gamma)$, and $\widetilde{J}=J(1+\eta)$ are impurity parameters. The nearest-neighbor interactions between the Ising and Heisenberg spins and the Ising-type exchange interaction of nodal spins are represented by J. Here we consider the case of ferromagnetic interactions ($J_{\rm H}>0$ and $J>0$) and a homogeneous magnetic field B applied along the z direction.

The cluster Hamiltonians commute with each other, $[H_j,H_k]=0$. Thus we can adopt the transfer-matrix approach to gain the partition function of the model with two impurities, which can be written as[38]

$$\begin{aligned}Z_N=&\sum_{\{\sigma\}}\omega(\sigma_{a,1}^z,\sigma_{b,1}^z,\sigma_{a,2}^z,\sigma_{b,2}^z)\cdots\widetilde{\omega}(\sigma_{a,r-1}^z,\sigma_{b,r-1}^z,\sigma_{a,r}^z,\sigma_{b,r}^z)\omega(\sigma_{a,r}^z,\sigma_{b,r}^z,\sigma_{a,r+1}^z,\sigma_{b,r+1}^z)\\&\times\widetilde{\omega}(\sigma_{a,r+1}^z,\sigma_{b,r+1}^z,\sigma_{a,r+2}^z,\sigma_{b,r+2}^z)\cdots\omega(\sigma_{a,N}^z,\sigma_{b,N}^z,\sigma_{a,1}^z,\sigma_{b,1}^z),\end{aligned} \tag{4}$$

where $\{\sigma\}$ represents all possible (4^N) spin arrangement. Here we consider the periodic boundary condition $\sigma^z_{a,N+1} = \sigma^z_{a,1}$ and $\sigma^z_{b,N+1} = \sigma^z_{b,1}$.

First one defines the four-qubit operator

$$V = \mathrm{e}^{-\beta H(\sigma^z_{a,i},\sigma^z_{b,i},\sigma^z_{a,i+1},\sigma^z_{b,i+1})} = \sum_{k=1}^{16} \mathrm{e}^{-\beta\varepsilon_k(\sigma^z_{a,i},\sigma^z_{b,i},\sigma^z_{a,i+1},\sigma^z_{b,i+1})}|\psi_k\rangle\langle\psi_k|, \tag{5}$$

where $\beta = 1/(k_{\mathrm{B}}T)$ and the Boltzmann's constant k_{B} is set to 1. In the basis $\{\sigma^z_{a,i},\sigma^z_{b,i},\sigma^z_{a,i+1},\sigma^z_{b,i+1}\}$ of the two consecutive blocks and $\sigma^z_{a(b),i} = \pm 1$, the transfer matrix W can be expressed as

$$W = \begin{pmatrix} \omega(\uparrow\uparrow\uparrow\uparrow) & \omega(\uparrow\uparrow\uparrow\downarrow) & \omega(\uparrow\uparrow\downarrow\uparrow) & \omega(\uparrow\uparrow\downarrow\downarrow) \\ \omega(\uparrow\downarrow\uparrow\uparrow) & \omega(\uparrow\downarrow\uparrow\downarrow) & \omega(\uparrow\downarrow\downarrow\uparrow) & \omega(\uparrow\downarrow\downarrow\downarrow) \\ \omega(\downarrow\uparrow\uparrow\uparrow) & \omega(\downarrow\uparrow\uparrow\downarrow) & \omega(\downarrow\uparrow\downarrow\uparrow) & \omega(\downarrow\uparrow\downarrow\downarrow) \\ \omega(\downarrow\downarrow\uparrow\uparrow) & \omega(\downarrow\downarrow\uparrow\downarrow) & \omega(\downarrow\downarrow\downarrow\uparrow) & \omega(\downarrow\downarrow\downarrow\downarrow) \end{pmatrix}, \tag{6}$$

where $\uparrow$ and $\downarrow$ denote the eigenvalues 1 and -1 of the Pauli matrix in the z direction, respectively. The element of W is called Boltzmann factor, which is written as

$$\omega(\sigma^z_{a,i},\sigma^z_{b,i},\sigma^z_{a,i+1},\sigma^z_{b,i+1}) = \sum_{k=1}^{16} \mathrm{e}^{-\beta\varepsilon_k(\sigma^z_{a,i},\sigma^z_{b,i},\sigma^z_{a,i+1},\sigma^z_{b,i+1})}. \tag{7}$$

Similarly, the transfer matrix for impurity is

$$\widetilde{W} = \begin{pmatrix} \widetilde{\omega}(\uparrow\uparrow\uparrow\uparrow) & \widetilde{\omega}(\uparrow\uparrow\uparrow\downarrow) & \widetilde{\omega}(\uparrow\uparrow\downarrow\uparrow) & \widetilde{\omega}(\uparrow\uparrow\downarrow\downarrow) \\ \widetilde{\omega}(\uparrow\downarrow\uparrow\uparrow) & \widetilde{\omega}(\uparrow\downarrow\uparrow\downarrow) & \widetilde{\omega}(\uparrow\downarrow\downarrow\uparrow) & \widetilde{\omega}(\uparrow\downarrow\downarrow\downarrow) \\ \widetilde{\omega}(\downarrow\uparrow\uparrow\uparrow) & \widetilde{\omega}(\downarrow\uparrow\uparrow\downarrow) & \widetilde{\omega}(\downarrow\uparrow\downarrow\uparrow) & \widetilde{\omega}(\downarrow\uparrow\downarrow\downarrow) \\ \widetilde{\omega}(\downarrow\downarrow\uparrow\uparrow) & \widetilde{\omega}(\downarrow\downarrow\uparrow\downarrow) & \widetilde{\omega}(\downarrow\downarrow\downarrow\uparrow) & \widetilde{\omega}(\downarrow\downarrow\downarrow\downarrow) \end{pmatrix}, \tag{8}$$

and the Boltzmann factor for impurity is given by the following expression:

$$\widetilde{\omega}(\sigma^z_{a,i},\sigma^z_{b,i},\sigma^z_{a,i+1},\sigma^z_{b,i+1}) = \sum_{k=1}^{16} \mathrm{e}^{-\beta\widetilde{\varepsilon}_k(\sigma^z_{a,i},\sigma^z_{b,i},\sigma^z_{a,i+1},\sigma^z_{b,i+1})}. \tag{9}$$

Then we can write the partition function of the butterfly-shaped chain with two impurities straightforwardly by

$$Z_N = \mathrm{tr}\,(\widetilde{W}W\widetilde{W}W^{N-3}). \tag{10}$$

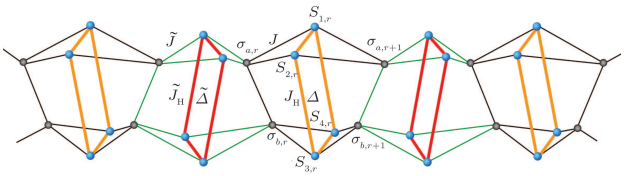


Fig. 1. A schematic representation of the spin-1/2 Ising–Heisenberg butterfly-shaped chain. The blue balls denote the Heisenberg particles and the red (orange) lines represent the Heisenberg interaction with (without) impurity, while the black balls denote the Ising spins and the green (black) lines represent the Ising interaction with (without) impurity.

By tracing out all Heisenberg spins except the Heisenberg spins at the r-th block on a butterfly-shaped chain, we can write the density operator as

$$\rho_{m,n} = \frac{1}{Z_N}\sum_{\{\sigma\}} \omega(\sigma^z_{a,1},\sigma^z_{b,1},\sigma^z_{a,2},\sigma^z_{b,2})\cdots\widetilde{\omega}(\sigma^z_{a,r-1},\sigma^z_{b,r-1},\sigma^z_{a,r},\sigma^z_{b,r})V_{m,n}(\sigma^z_{a,r},\sigma^z_{b,r},\sigma^z_{a,r+1},\sigma^z_{b,r+1}) \times \widetilde{\omega}(\sigma^z_{a,r+1},\sigma^z_{b,r+1},\sigma^z_{a,r+2},\sigma^z_{b,r+2})\cdots\omega(\sigma^z_{a,N},\sigma^z_{b,N},\sigma^z_{a,1},\sigma^z_{b,1}). \tag{11}$$

And, we can also write the density operator straightforwardly as

$$\rho_{m,n} = \frac{1}{Z_N}\mathrm{tr}\,(W^{r-2}\widetilde{W}P_{m,n}\widetilde{W}W^{N-r-1}) = \frac{1}{Z_N}\mathrm{tr}\,(\widetilde{W}P_{m,n}\widetilde{W}W^{N-3}), \tag{12}$$

where

$$P_{m,n} = \begin{pmatrix} V_{m,n}(\uparrow\uparrow\uparrow\uparrow) & V_{m,n}(\uparrow\uparrow\uparrow\downarrow) & V_{m,n}(\uparrow\uparrow\downarrow\uparrow) & V_{m,n}(\uparrow\uparrow\downarrow\downarrow) \\ V_{m,n}(\uparrow\downarrow\uparrow\uparrow) & V_{m,n}(\uparrow\downarrow\uparrow\downarrow) & V_{m,n}(\uparrow\downarrow\downarrow\uparrow) & V_{m,n}(\uparrow\downarrow\downarrow\downarrow) \\ V_{m,n}(\downarrow\uparrow\uparrow\uparrow) & V_{m,n}(\downarrow\uparrow\uparrow\downarrow) & V_{m,n}(\downarrow\uparrow\downarrow\uparrow) & V_{m,n}(\downarrow\uparrow\downarrow\downarrow) \\ V_{m,n}(\downarrow\downarrow\uparrow\uparrow) & V_{m,n}(\downarrow\downarrow\uparrow\downarrow) & V_{m,n}(\downarrow\downarrow\downarrow\uparrow) & V_{m,n}(\downarrow\downarrow\downarrow\downarrow) \end{pmatrix}. \tag{13}$$

Diagonalizing the transfer matrix W^{N-3} by using the matrix U, we can give

$$\Lambda^{N-3} = \begin{pmatrix} \lambda_1^{N-3} & 0 & 0 & 0 \\ 0 & \lambda_2^{N-3} & 0 & 0 \\ 0 & 0 & \lambda_3^{N-3} & 0 \\ 0 & 0 & 0 & \lambda_4^{N-3} \end{pmatrix}. \tag{14}$$

The density operator can be finally expressed by

$$\rho_{m,n} = \frac{\mathrm{tr}\,(U^{-1}\widetilde{W}P_{m,n}\widetilde{W}U\Lambda^{N-3})}{\mathrm{tr}\,(\widetilde{W}W\widetilde{W}U\Lambda^{N-3}U^{-1})}. \tag{15}$$

This result is valid for arbitrary number N of blocks in the butterfly-shaped chain under the periodic boundary conditions. Now considering the thermodynamic limit $N \to \infty$ and $(\lambda_{2(3,4)}/\lambda_1)^{N-3} \to 0$, the density operator becomes

$$\rho_{m,n} = \frac{\mathrm{tr}\left(U^{-1}\widetilde{W}P_{m,n}\widetilde{W}U\begin{pmatrix} 1&0&0&0\\0&0&0&0\\0&0&0&0\\0&0&0&0\end{pmatrix}\right)}{\mathrm{tr}\left(\widetilde{W}W\widetilde{W}U\begin{pmatrix} 1&0&0&0\\0&0&0&0\\0&0&0&0\\0&0&0&0\end{pmatrix}U^{-1}\right)}. \tag{16}$$

Thus we can compute the reduced density matrix by tracing out the density operator. The reduced density operator for the

subsystem AB is defined by

$$\rho^{AB} = \mathrm{tr}_{CD}(\rho^{ABCD}), \tag{17}$$

where tr_{CD} is known as the partial trace over the system CD.

3. Results and discussion

In this section, we study the entanglement of two Heisenberg spins in the r-th block of the spin-1/2 Ising–Heisenberg butterfly-shaped model. By calculating the thermal entanglement of the nearest-neighbor and the next-nearest neighbor Heisenberg spins, we compare the results of the butterfly-shaped model with two impurities on the $(r-1)$-th and the $(r+1)$-th blocks and the clean model firstly. Then we give the entanglement calculation of the random fluctuation of the two impurities which follow the uniform distribution and the Gaussian distribution respectively.

The entanglement between the two Heisenberg spins, which interact with two Ising spins respectively, has a quantitative definition of concurrence as the most basic entanglement measure. It is defined as[16,18]

$$C(\rho) = \max\{\sqrt{\lambda_1} - \sqrt{\lambda_2} - \sqrt{\lambda_3} - \sqrt{\lambda_4}, 0\}, \tag{18}$$

where $\lambda_1 \geqslant \lambda_2 \geqslant \lambda_3 \geqslant \lambda_4$ are the eigenvalues of the operator

$$R = \rho(\sigma^y \otimes \sigma^y)\rho^*(\sigma^y \otimes \sigma^y), \tag{19}$$

with ρ^* being the complex conjugate of the reduced density matrix ρ. The concurrence $C = 0$ corresponds to an unentangled state, while $C = 1$ corresponds to a maximally entangled state.

3.1. Spin chain with two impurities

After numerical solving Eq. (16) to gain the density matrix, we can calculate the reduced density matrix of the model and further obtain the concurrence of the entanglement measure between the two Heisenberg spins according to Eq. (18). The concurrences of the nearest-neighbor and the next-nearest neighbor Heisenberg spins are denoted by C_{12} and C_{13}, respectively.

In Fig. 2, we plot that the concurrence C_{12} varies with the impurity parameter η for different values of Δ. It is shown that a sharp variation of the concurrence occurs with η. For example, in the case with $\Delta = 0.2$, the concurrence remains at the maximum $C_{12}^{\max} \approx 0.5$ for $\eta \lesssim -0.04$, when $\eta > -0.04$, C_{12} decreases (*i.e.*, for $\eta = 0$, $C_{12} \approx 0.487$), and it descended to a stable value $C_{12} \approx 0.23$ when $\eta \gtrsim 0.09$. As the anisotropic parameter increases, for the values of $\Delta = 0.4$ and 0.5, entanglement death occurs when $\eta \gtrsim -0.27$ and $\eta \gtrsim -0.36$ respectively. The variations of concurrence C_{13} with the impurity parameter η for different values of Δ are similar to those of concurrence C_{12}. Here we consider a fixed magnetic field. It is also necessary to indicate that $0 \leqslant \Delta \lesssim 0.55$ is the region where the entanglement occurs within the range of $-0.9 \lesssim \eta \lesssim -0.4$.

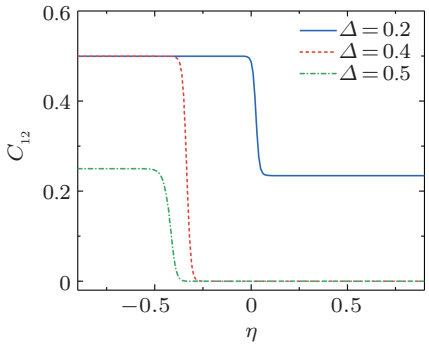


Fig. 2. Concurrence C_{12} as a function of the impurity parameter η for different values of Δ. Here, $J_{\mathrm{H}} = 2J$, $J = 1$, $T = 0.1$, $B = 4$, $\alpha = 0$, and $\gamma = 0.5$.

The concurrence C_{12} as a function of the external magnetic field B is shown in Figs. 3(a) and 3(b) for different values of temperature T. The solid and dot lines correspond to the clean model and the two-impurity model, respectively. In Fig. 3(a), we plot the behavior of C_{12} for $\Delta = 0.4$. When the external magnetic field B increases, the concurrence of the clean model first increases from zero to the maximum and then decreases to zero. In the case of $T = 0.1$, the concurrence begins to appear at $B \approx 1.16$ and achieves the maximum value of $C_{12}^{\max} = 0.5$ within the region $2.2 \lesssim B \lesssim 2.5$, then goes down to zero at $B \approx 3.74$. Different from the clean model, with increasing the magnetic field, the entanglement behavior of the two-impurity chain model is more robust. In the two-impurity model, when the magnetic field B increases, it is interesting to observe that the concurrence first increases from zero to the maximum value, then decreases to a certain value, and starts to go up to the second peak, and ultimately goes down to zero. The case of $\Delta = 0.5$ is shown in Fig. 3(b). It is shown that the two-impurity model displays the phenomenon of entanglement revival at a low temperature (*e.g.*, $T = 0.1$).

We plot the concurrence C_{13} as a function of the external magnetic field B for different values of temperature T in Figs. 3(c) and 3(d). The case with $\Delta = 0.4$ is shown in Fig. 3(c). For the clean model, with the magnetic field strength increasing, the concurrence decreases from the initial value to $C_{13} \approx 0.106$, then gradually increases to the maximum value, and decreases to zero finally. While for the two-impurity model there are two peaks in the curve of the concurrence C_{13}, and the maximum value of concurrence appears in the second peak under a larger magnetic field. For the case $\Delta = 0.5$ and $T = 0.5$ in Fig. 3(d), with the increase of the magnetic field strength, the concurrence decreases from the initial value to zero, and the entanglement revival occurs subsequently for both two models. However, for the lower temperature (see the case of $T = 0.1$), the entanglement revival occurs twice for the two-impurity model, and the concurrence reaches the maximum value $C_{13}^{\max} \approx 0.47$ at $B \approx 3.79$, while for the clean

model the increasing of the magnetic field suppresses the entanglement.

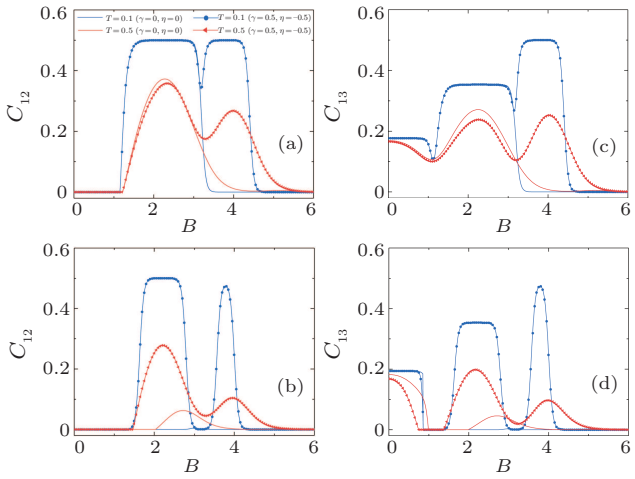


Fig. 3. Concurrences C_{12} and C_{13} as a function of the external magnetic field B for different values of temperature T. Here, $J_{\rm H} = 2J$, $J = 1$, and $\alpha = 0$. In panels (a) and (c) we display concurrence for $\Delta = 0.4$, panels (b) and (d) for $\Delta = 0.5$. The solid lines and dot lines correspond to the clean model and the two-impurity model, respectively.

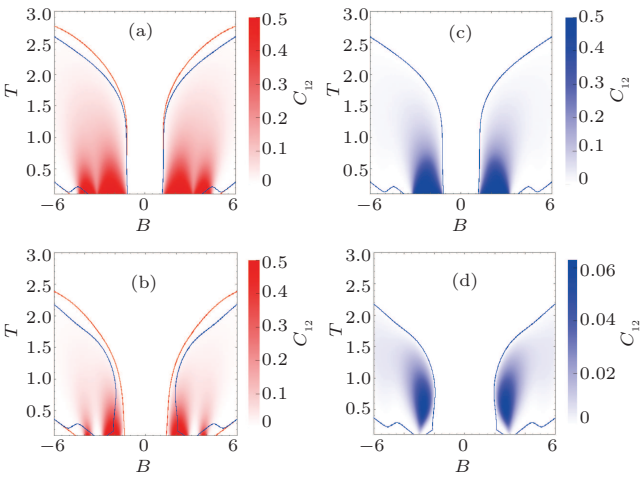


Fig. 4. Density plot of concurrence C_{12} as a function of the external magnetic field B and temperature T with $J_{\rm H} = 2J$ and $J = 1$. In panels (a) and (b) we display C_{12} for the model with two impurities, where $\alpha = 0$, $\gamma = 0.5$, and $\eta = -0.5$. In panels (c) and (d) we display C_{12} for the clean model, where $\alpha = 0$, $\gamma = 0$, and $\eta = 0$. We set $\Delta = 0.4$ in panels (a) and (c), $\Delta = 0.5$ in panels (b) and (d), respectively. The red and blue solid curves are the contours of $C_{12} = 0$ which correspond to the two-impurity model and the clean model, respectively.

Figure 4 shows the density plot of the concurrence C_{12} as a function of external magnetic field B and temperature T. In Figs. 4(a) and 4(b), the red areas indicate the presence of entanglement and the white areas indicate the absence of entanglement of the two-impurity model. For the convenience of comparison, the entanglement disappearance boundary of the two-impurity model is represented by red line, and the entanglement disappearance boundary of the clean model is also given by blue line. The blue entangled and white unentangled regions of the clean model are plotted in Figs. 4(c) and 4(d). It is shown that the entangled region of the two-impurity model is larger than the region of clean model.

In Fig. 5 we display the density plot of the concurrence C_{13} as a function of the external magnetic field B and temperature T. Clearly, the maximum concurrence value of the two-impurity model is greater than that of the clean model. When the anisotropic parameter $\Delta = 0.4$, as shown in Fig. 5(a), the maximum concurrence value of the two-impurity model $C_{13}^{\max} \approx 0.4999$, and that of the clean model $C_{13}^{\max} \approx 0.35$ as shown in Fig. 5(c). As $\Delta = 0.5$, the maximum concurrence value of the two-impurity model $C_{13}^{\max} \approx 0.47$ in Fig. 5(b), whereas that of the clean model $C_{13}^{\max} \approx 0.19$ as shown in Fig. 5(d).

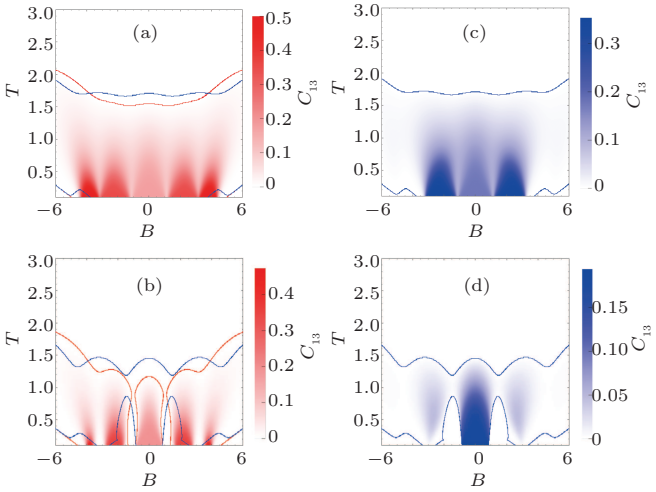


Fig. 5. Density plot of concurrence C_{13} as a function of the external magnetic field B and temperature T with $J_{\rm H} = 2J$ and $J = 1$. In panels (a) and (b) we display C_{13} for the model with two impurities, where $\alpha = 0$, $\gamma = 0.5$, and $\eta = -0.5$. In panels (c) and (d) we display C_{13} for the clean model, where $\alpha = 0$, $\gamma = 0$, and $\eta = 0$. We set $\Delta = 0.4$ in panels (a) and (c), $\Delta = 0.5$ in panels (b) and (d), respectively. The red and blue solid curves are the contours of $C_{13} = 0$ which correspond to the two-impurity model and the clean model, respectively.

3.2. Two impurities with fluctuation

In this subsection, we illustrate the influence of impurity fluctuations on thermal entanglement in the two-impurity model. Taking $\gamma = 0.5$ and $\eta = -0.5$ as the mean values, we discuss the two cases where the impurity parameters γ and η submit to the uniform distribution and the Gaussian distribution, respectively.

In Figs. 6(a) and 6(b), we show the effect of the external magnetic field with uniformly distributed impurity parameters on the concurrence C_{12}. Here we take $T = 0.1$ as an example. In Fig. 6(a) (the case of $\Delta = 0.4$), with the increasing of the magnetic field B, the entanglement appears at $B \approx 1.13$, and achieves the maximum concurrence value $C_{12}^{\max} \approx 0.467$ when $B \approx 2.65$, and disappears at $B \approx 4.69$. In Fig. 6(b) (the case of $\Delta = 0.5$), the entanglement appears at $B \approx 1.06$, and achieves the maximum concurrence value $C_{12}^{\max} \approx 0.379$ when $B \approx 2.58$. Then the entanglement decreases nonmonotonically and finally disappears at $B \approx 4.27$. In Figs. 6(c) and 6(d), we show the effect of the magnetic field with the Gaussian distributed impurity parameters on the concurrence C_{12}. When $\Delta = 0.4$,

there are two peaks and the magnetic field region of the entanglement occurring is $1.16 \lesssim B \lesssim 4.71$. The maximum concurrence value $C_{12}^{\max} \approx 0.4983$ happens at $B \approx 2$. For the case of $\Delta = 0.5$, the maximum concurrence value $C_{12}^{\max} \approx 0.4938$ at $B \approx 2.4$ and the second peak occurs in the area where the magnetic field is $3 \lesssim B \lesssim 4.3$.

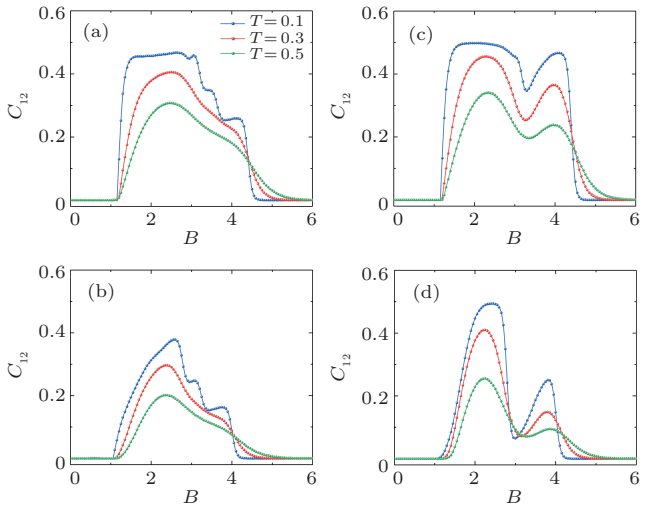


Fig. 6. The concurrence C_{12} as a function of the external magnetic field B under different values of temperature T with impurity fluctuations. Here, $J_{\mathrm{H}} = 2J$, $J = 1$ and $\alpha = 0$. In panels (a) and (b) we present the uniform distribution for two impurities, and the Gaussian distribution in panels (c) and (d). For panels (a) and (c) $\Delta = 0.4$, panels (b) and (d) $\Delta = 0.5$. We take the average of 1000 calculations here.

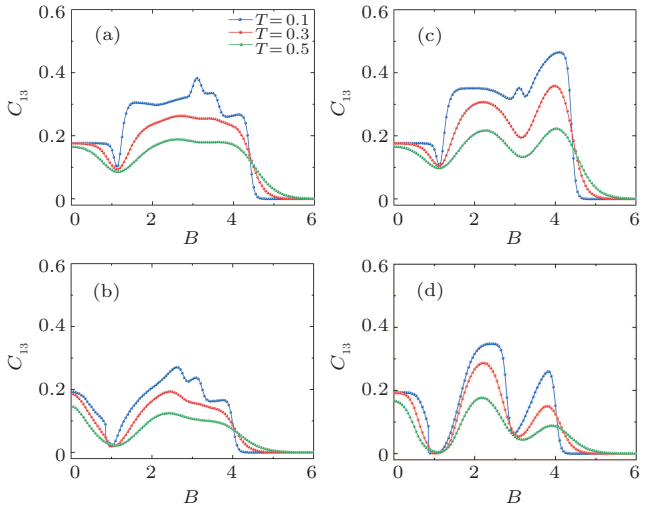


Fig. 7. The concurrence C_{13} as a function of the external magnetic field B under different values of temperature T with impurity fluctuations. Here, $J_{\mathrm{H}} = 2J$, $J = 1$ and $\alpha = 0$. In panels (a) and (b) we present the uniform distribution for two impurities, and the Gaussian distribution in panels (c) and (d). For panels (a) and (c) $\Delta = 0.4$, panels (b) and (d) $\Delta = 0.5$. We take the average of 1000 calculations here.

The influence of impurity fluctuations with uniformly distributed impurity parameters on the concurrence C_{13} is presented in Figs. 7(a) and 7(b). Let us consider the case $T = 0.1$. When $\Delta = 0.4$, as shown in Fig. 7(a), the region of the magnetic field of the entanglement occurring is $0 \leqslant B \lesssim 4.69$, and the maximum concurrence value $C_{13}^{\max} \approx 0.3825$ at $B \approx 3.1$. It is less than $C_{13}^{\max} \approx 0.4999$ of the two-impurity model but greater than $C_{13}^{\max} \approx 0.3535$ of the clean model. In the case of $\Delta = 0.5$, as shown in Fig. 7(b), the magnetic field region of the entanglement occurring is $0 \leqslant B \lesssim 4.27$, and the maximum concurrence value $C_{13}^{\max} \approx 0.271$ at $B \approx 2.62$. The case of the Gaussian distribution is shown in Figs. 7(c) and 7(d). When $\Delta = 0.4$, a special small peak appears at magnetic field $B \approx 3.1$, and the maximum concurrence value $C_{13}^{\max} \approx 0.465$ at $B \approx 4.11$. When $\Delta = 0.5$, with the increasing of the magnetic field, the concurrence decreases from the initial value of 0.194 to $C \approx 0.01$, and then begins to recover. After going through two peaks, the concurrence decreases to 0, and the maximum concurrence value $C_{13}^{\max} \approx 0.348$ at $B \approx 2.39$.

It is worth mentioning that compared with the case of the clean model, in the two cases of the impurity fluctuations with the uniform and the Gaussian distributions, the regions of the magnetic field where the entanglement occurs are broadened for both C_{12} and C_{13}.

4. Conclusions

In this paper, we investigated the thermal entanglement properties in a spin-1/2 Ising–Heisenberg butterfly-shaped chain with impurities. Based on the transfer-matrix approach, we numerically calculated the concurrence C_{12} between the nearest-neighbor Heisenberg spins and C_{13} between the next-nearest neighbor Heisenberg spins of the r-th block in the model. The thermal entanglement of the two-impurity model and the clean model were discussed, respectively. Firstly, we studied the variations of the concurrence with the impurity parameter η for different values of Δ, and obtained the appropriate region of the impurity and anisotropic parameters where the entanglement occurs in a certain magnetic field. Then, we investigated the effect of the external magnetic field B on the entanglement. It is shown that the two-impurity model can broaden the magnetic field region where the entanglement occurs and enlarge the maximum concurrence value within a certain anisotropic parameter range. It is also found that the entanglement decreases as the value of temperature increases. Finally, the effect of the fluctuation of impurity parameters in the two-impurity model on the thermal entanglement is given. By considering the uniform distribution and the Gaussian distribution of impurity parameters, it can be concluded that due to the fluctuation of impurity, the magnetic field region entanglement occurring becomes wider and the entanglement behavior becomes more robust.

It would be interesting to note that one-dimensional spin-1/2 entangled chains are considered to act as channels for long-distance and high-fidelity quantum teleportation.[45,47] For a random spin chain, the probability of obtaining a spin pair with higher fidelity and greater entanglement would be increased by using defects.

References

[1] Bell J S 1987 *Speakable and unspeakable in quantum mechanics* (Cambridge: Cambridge University)
[2] Peres A 2006 *Quantum theory: concepts and methods* (Springer Science & Business Media)
[3] Bennett C H, Brassard G, Crépeau C, Jozsa R, Peres A and Wootters W K 1993 *Phys. Rev. Lett.* **70** 1895
[4] Boschi D, Branca S, de Martini F, Hardy L and Popescu S 1998 *Phys. Rev. Lett.* **80** 1121
[5] Venuti L C, Giampaolo S, Illuminati F and Zanardi P 2007 *Phys. Rev. A* **76** 052328
[6] Bennett C H 1992 *Phys. Rev. Lett.* **68** 3121
[7] Shor P W and Preskill J 2000 *Phys. Rev. Lett.* **85** 441
[8] Lo H K, Ma X and Chen K 2005 *Phys. Rev. Lett.* **94** 230504
[9] Gisin N and Massar S 1997 *Phys. Rev. Lett.* **79** 2153
[10] Scarani V, Iblisdir S, Gisin N and Acin A 2005 *Rev. Mod. Phys.* **77** 1225
[11] Wang M H and Cai Q Y 2019 *Phys. Rev. A* **99** 012324
[12] Wang X 2002 *Phys. Rev. A* **66** 034302
[13] Zhou L, Song H S, Guo Y Q and Li C 2003 *Phys. Rev. A* **68** 024301
[14] Zhang G F and Li S S 2005 *Phys. Rev. A* **72** 034302
[15] Vedral V, Plenio M B, Rippin M A and Knight P L 1997 *Phys. Rev. Lett.* **78** 2275
[16] Hill S and Wootters W K 1997 *Phys. Rev. Lett.* **78** 5022
[17] Plenio M B and Vedral V 1998 *Contemp. Phys.* **39** 431
[18] Wootters W K 1998 *Phys. Rev. Lett.* **80** 2245
[19] Coffman V, Kundu J and Wootters W K 1999 *Phys. Rev. A* **61** 052306
[20] Gunlycke D, Kendon V, Vedral V and Bose S 2001 *Phys. Rev. A* **64** 042302
[21] Wang X 2001 *Phys. Rev. A* **64** 012313
[22] Kargarian M, Jafari R and Langari A 2008 *Phys. Rev. A* **77** 032346
[23] Amico L, Fazio R, Osterloh A and Vedral V 2008 *Rev. Mod. Phys.* **80** 517
[24] Bethe H 1931 *Z. Phys.* **71** 205
[25] Baxter R J 1982 *Exactly solved models in statistical mechanics* (New York: Academic Press)
[26] Yeomans J M 1992 *Statistical mechanics of phase transitions* (Clarendon Press)
[27] Rommer S and Eggert S 1999 *Phys. Rev. B* **59** 6301
[28] Osenda O, Huang Z and Kais S 2003 *Phys. Rev. A* **67** 062321
[29] Santos L F 2003 *Phys. Rev. A* **67** 062306
[30] Apollaro T J and Plastina F 2006 *Phys. Rev. A* **74** 062316
[31] Huang Z, Osenda O and Kais S 2004 *Phys. Lett. A* **322** 137
[32] Cai J M, Zhou Z W and Guo G C 2006 *Phys. Lett. A* **352** 196
[33] Hoyos J A and Rigolin G 2006 *Phys. Rev. A* **74** 062324
[34] Rule K C, Reehuis M, Gibson M C R, Ouladdiaf B, Gutmann M J, Hoffmann J U, Gerischer S, Tennant D A, Süllow S and Lang M 2011 *Phys. Rev. B* **83** 104401
[35] Jeschke H, Opahle I, Kandpal H, Valentí R, Das H, Saha-Dasgupta T, Janson O, Rosner H, Brühl A, Wolf B, Lang M, Richter J, Hu S, Wang X, Peters R, Pruschke T and Honecker A 2011 *Phys. Rev. Lett.* **106** 217201
[36] Qiao J and Zhou B 2015 *Chin. Phys. B* **24** 110306
[37] Zheng Y D, Mao Z and Zhou B 2017 *Chin. Phys. B* **26** 070302
[38] Rojas O, Rojas M, Ananikian N S and de Souza S M 2012 *Phys. Rev. A* **86** 042330
[39] Rojas O, Rojas M, de Souza S M, Torrico J, Strečka J and Lyra M L 2017 *Physica A* **486** 367
[40] Verkholyak T and Strečka J 2013 *Phys. Rev. B* **88** 134419
[41] Rojas O, Strečka J and Lyra M L 2013 *Phys. Lett. A* **377** 920
[42] Strečka J, Rojas O, Verkholyak T and Lyra M L 2014 *Phys. Rev. E* **89** 022143
[43] Karl'ová K, Strečka J and Lyra M L 2018 *Phys. Rev. B* **97** 104407
[44] Carvalho I M, Rojas O, de Souza S M and Rojas M 2019 *Quantum Inf. Process.* **18** 134
[45] Freitas M, Filgueiras C and Rojas M 2019 *Ann. Phys.* **531** 1900261
[46] Zad H A, Ananikian N and Kenna R 2019 *J. Phys.: Condens. Matter* **31** 445802
[47] Zheng Y D, Mao Z and Zhou B 2019 *Chin. Phys. B* **28** 120307